J|A|C|S ARTICLES

Published on Web 02/18/2009

Macrocyclic Receptor Exhibiting Unprecedented Selectivity for Light Lanthanides

Adrián Roca-Sabio,[†] Marta Mato-Iglesias,[†] David Esteban-Gómez,[†] Éva Tóth,[‡] Andrés de Blas,[†] Carlos Platas-Iglesias,*[,†] and Teresa Rodríguez-Blas*[,†]

Departamento de Química Fundamental, Universidade da Coruña, Campus da Zapateira, Alejandro de la Sota 1, 15008 A Coruña, Spain, and Centre de Biophysique Moléculaire, CNRS, rue Charles Sadron, 45071 Orléans, Cedex 2, France

Received November 4, 2008; E-mail: cplatas@udc.es (C.P.-I.); mayter@udc.es (T.R.-B.)

Abstract: We report a new macrocyclic ligand, *N,N′*-bis[(6-carboxy-2-pyridil)methyl]-4,13-diaza-18-crown-6 (H_2bp18c6), designed for complexation of lanthanide ions in aqueous solution. Potentiometric measurements evidence an unprecedented selectivity of bp18c6 for the large Ln^{III} ions. Among the different Ln^{III} ions, La^{III} and Ce^{III} show the highest log K_{ML} values, with a dramatic drop of the stability observed from Ce^{III} to Lu^{III} as the ionic radius of the Ln^{III} ions decreases (log K_{CeL} − log K_{LuL} = 6.9). The X-ray crystal structures of the Gd^{III} and Yb^{III} complexes show that the metal ion is directly bound to the 10 donor atoms of the bp18c6 ligand. The structure of the complexes in solution has been investigated by ^{1}H and ^{13}C NMR spectroscopy, as well as by theoretical calculations performed at the DFT (B3LYP) level. Our results indicate that a conformational change occurs around the middle of the lanthanide series: for the larger Ln^{III} ions the most stable conformation is $\Delta(\delta\lambda\delta)(\delta\lambda\delta)$, while for the smallest Ln^{III} ions (Gd−Lu) our calculations predict the $\Delta(\lambda\delta\lambda)(\lambda\delta\lambda)$ form being the most stable one. This structural change was confirmed by the analysis of the Ce^{III}-, Pr^{III}-, and Yb^{III}-induced paramagnetic ^{1}H shifts. The selectivity that bp18c6 shows for the large Ln^{III} ions can be attributed to a better fit between the light Ln^{III} ions and the relatively large crown fragment of the ligand. Indeed, our DFT calculations indicate that the interaction between the Ln^{III} ion and several donor atoms of the crown moiety is weakened as the ionic radius of the metal ion decreases.

Introduction

Highly selective separation of lanthanides is very important in high-technology industry because of the unique electronic, magnetic, and optical properties of this series of elements.[1] Effective methods for the separation and purification of lanthanides are also of interest for the design of radiopharmaceuticals for the treatment of various diseases involving cancer.[2] However, it is widely recognized that the separation of lanthanides into individual elements is rather difficult because of their similar physical and chemical properties, which is the major reason why lanthanides are expensive.[3] As far as coordination chemistry is concerned, the main difference between the Ln^{III} ions is the small monotonous contraction of the ionic radius upon increasing atomic number.[4] However, the overall relative contraction of ionic radius on going from La^{III} to Lu^{III} amounts only to ca. 16%. Thus, the design of systems that can selectively recognize a given Ln^{III} ion, or at least a particular group of them, remains a challenging task for coordination chemistry.[5]

The stability trends for Ln^{III} complexes in aqueous solution usually fall within one of the following categories: (i) in the most common case, the stability constants increase from La^{III} to Lu^{III} due to the increase of charge density of the metal ions;[6] (ii) the stability increases across the series, reaches a plateau, and then declines;[7] (iii) with very few ligands, the stability decreases along the lanthanide series.[8] However, independently of the stability trend, most of ligands provide limited discrimination along the lanthanide series, except for a few cases where an important selectivity was found for the heavier lanthanides.[6]

The cyclic framework of crown ethers affords an interesting platform for the complexation of metal ions, and in particular, the hard acid character of the crown moiety makes crown ethers interesting potential ligands for the complexation of trivalent

[†] Universidade da Coruña.
[‡] Centre de Biophysique Molèculaire.

(1) Bünzli, J.-C. G.; Choppin, G. R. In *Lanthanide Probed in Life, Chemical and Earth Sciences*; Bünzli, J.-C. G., Choppin, G. R., Eds.; Elsevier: Amsterdam, 1989.
(2) (a) Chauvin, A.-S.; Bünzli, J. -C. G.; Bochud, F.; Scopelliti, R.; Froidevaux, P. *Chem. Eur. J.* **2006**, *12*, 6852–6864. (b) Kala, R.; Gladis, J. M.; Rao, T. P. *Anal. Chim. Acta* **2004**, *518*, 143–150.
(3) Nash, K. L.; Jensen, M. P. In *Handbook on the Physics and Chemistry of Rare Earths*; Gschneidner, J. K. A., Eyring, L., Eds.; Elsevier: Amsterdam, 2000; Vol. 28, pp 311−371.
(4) Seitz, M.; Oliver, A. G.; Raymond, K. N. *J. Am. Chem. Soc.* **2007**, *129*, 11153–11160.
(5) (a) André, N.; Scopelliti, R.; Hopfgartner, G.; Piguet, C.; Bünzli, J.-C. G. *Chem. Commun.* **2002**, 214–215. (b) Piguet, C.; Bünzli, J.-C. G. *Chem. Soc. Rev.* **1999**, *28*, 347–358. (c) Floquet, S.; Borkovec, M.; Bernardinelli, G.; Pinto, A.; Leuthold, L.-A.; Hopfgartner, G.; Imbert, D.; Bünzli, J.-C. G.; Piguet, C. *Chem. Eur. J.* **2004**, *10*, 1091–1105.
(6) (a) Caravan, P.; Hedlund, T.; Liu, S.; Sjöberg, S.; Orvig, C. *J. Am. Chem. Soc.* **1995**, *117*, 11230–11238. (b) Chapon, D.; Morel, J.-P.; Delangle, P.; Gateau, C.; Pécaut, J. *Dalton Trans* **2003**, 2745–2749.
(7) Sarka, L.; Bányai, I.; Brücher, E.; Király, R.; Platzek, J.; Radüchel, B.; Schmitt-Willich, H. *J. Chem. Soc., Dalton Trans.* **2000**, 3699–3703.
(8) Chang, C. A.; Rowland, M. E. *Inorg. Chem.* **1983**, *22*, 3866–3869.

Chart 1

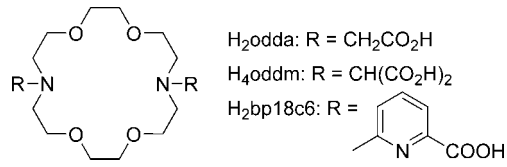

lanthanide ions.[9] Moreover, the relative facility with which crown ethers can be functionalized with pendant arm(s) containing additional donor atom(s) allows to enhance the cation binding ability and the selectivity of the parent crown ether.[10,11] The 18-membered ring of 4,13-diaza-18-crown-6 is known to be a useful platform for the design of selective ligands for large metal ions such as Ln^{III} ions. Indeed, the 4,13-bis(acetic acid) derivative odda (Chart 1) shows a certain degree of selectivity for the large Ln^{III} ions, and as a result, the stability constants of the $[Ln(odda)]^+$ complexes decrease slightly from Gd^{III} to Lu^{III}.[8] A more important drop of the stability constants across the lanthanide series is observed for the corresponding 7,16-bis(malonic acid) derivative oddm (Chart 1). In the latter case, the stability constants decrease by about 5 orders of magnitude form Ce^{III} to Lu^{III}.[12] However, the practical application of oddm is limited by the slow formation kinetics of the $[Ln(oddm)]^-$ complexes.

In recent papers we have reported a new series of octadentate acyclic ligands containing picolinate units and carboxylate[13] or phosphonate[14,15] pendants that were designed for stable Ln^{III} complexation in aqueous solution.[16] As a continuation of these works, we decided to exploit the favorable coordination properties toward the Ln^{III} ions of the picolinate groups, together with the selectivity that 4,13-diaza-18-crown-6 derivatives show for large metal ions, to design new ligands with potential application in Ln^{III} separation technologies. Thus, in this paper we report the macrocyclic ligand *N*,*N*′-bis[(6-carboxy-2-pyridil)methyl]-1,7-diaza-18-crown-6 (H_2bp18c6, Chart 1). We expected that the introduction of rigid picolinate pendants into the 4,13-diaza-18-crown-6 framework could provide a good selectivity of bp18c6 toward the largest Ln^{III} ions. Thermodynamic stability constants of the Ln^{III} complexes of this ligand have been determined by pH potentiometry. Aiming to rationalize the stability trend observed across the lanthanide series the structure of the Ln^{III} complexes was studied by using ^1H and ^{13}C NMR techniques in D_2O solution. In addition, the complexes were characterized by density functional theory (DFT) calculations carried out at the B3LYP level. The structures established by these calculations were compared with the structural information obtained in solution from paramagnetic NMR measurements (Ln^{III}-induced ^1H NMR shifts). The single-crystal X-ray structures of the Gd^{III} and Yb^{III} complexes are also reported.

Scheme 1. Synthesis of Ligand H_2bp18c6 and Its Numbering Scheme for NMR Spectral Assignment[a]

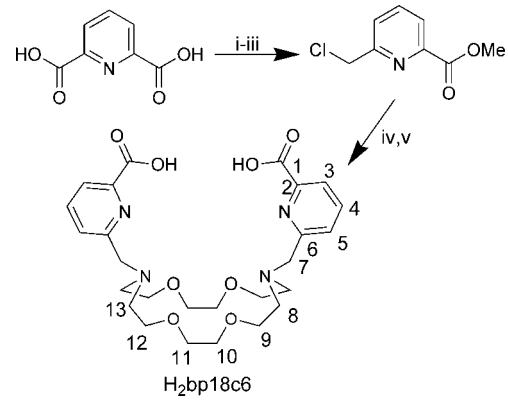

[a] (i) MeOH, H_2SO_4; (ii) $NaBH_4$, MeOH; (iii) $SOCl_2$; (iv) 4,13-diaza-18-crown-6, Na_2CO_3, CH_3CN; (v) HCl (6 M).

Results

Synthesis of the Ligand. The decadentate receptor H_2bp18c6 is readily obtained in five steps from commercially available pyridine-2,6-dicarboxylic acid and 4,13-diaza-18-crown-6 (Scheme 1). 6-Chloromethylpyridine-2-carboxylic acid methyl esther was prepared in good yield by partial reduction of dimethylpyridine-2,6-dicarboxylate followed by reaction with $SOCl_2$. Alkylation of 4,13-diaza-18-crown-6 with this chloromethyl derivative in refluxing acetonitrile in the presence of Na_2CO_3, and subsequent deprotection of the methyl esters with 6 M HCl yield the desired ligand H_2bp18c6.

Ligand Protonation Constants and Stability Constants of the Lanthanide Complexes. The protonation constants of bp18c6 and the stability constants of its metal complexes formed with Ln^{III} ions were determined by potentiometric titration; the constants and standard deviations are given in Table 1, which also lists the protonation constants of odda and oddm (Chart 1) and the stability constants of their Ln^{III} complexes. The ligand protonation constants are defined as in eq 1, and the stability constants of the metal chelates and the protonation constants of the complexes are expressed in eqs 2 and 3, respectively.

$$K_i = \frac{[H_iL]}{[H_{i-1}L][H^+]} \quad (1)$$

$$K_{ML} = \frac{[ML]}{[M][L]} \quad (2)$$

$$K_{MHL} = \frac{[MHL]}{[ML][H^+]} \quad (3)$$

In comparison to odda and oddm, bp18c6 has lower protonation constants for the first and second protonation steps, which occur on the amine nitrogen atoms. Thus, replacement of the acetate or malonate pendants by 6-methyl-2-pyridinecarboxylate groups leads to an important decrease in the basicity of the two

(9) Liu, Y.; Han, B.-H.; Li, Y.-M.; Chen, R.-T.; Ouchi, M.; Inoue, Y. *J. Chem. Phys.* **1996**, *100*, 17361–17364.
(10) Gokel, G. W.; Korzeniowski, S. H. *Macrocyclic Polyether Synthesis*; Springer: Berlin, 1982.
(11) Nakatsuji, Y.; Nakamura, T.; Yometani, M.; Yuya, H.; Okahara, M. *J. Am. Chem. Soc.* **1988**, *110*, 531–538.
(12) Brücher, E.; Györi, B.; Emri, J.; Solymosi, P.; Sztanyik, L. B.; Varga, L. *J. Chem. Soc., Chem. Commun.* **1993**, 574–575.
(13) Platas-Iglesias, C.; Mato-Iglesias, M.; Djanashvili, K.; Muller, R. N.; Vander Elst, L.; Peters, J. A.; de Blas, A.; Rodríguez-Blas, T. *Chem.-Eur. J.* **2004**, *10*, 3579–3590.
(14) Mato-Iglesias, M.; Platas-Iglesias, C.; Djanashvili, K.; Peters, J. A.; Tóth, É.; Balogh, E.; Muller, R. N.; Vander Elst, L.; de Blas, A.; Rodríguez-Blas, T. *Chem. Commun.* **2005**, 4729–4731.
(15) Balogh, E.; Mato-Iglesias, M.; Platas-Iglesias, C.; Tóth, É.; Djanashvili, K.; Peters, J. A.; de Blas, A.; Rodríguez-Blas, T. *Inorg. Chem.* **2006**, *45*, 8719–8728.
(16) Mato-Iglesias, M.; Balogh, E.; Platas-Iglesias, C.; Tóth, É.; de Blas, A.; Rodríguez-Blas, T. *Dalton Trans.* **2006**, 5404–5415.
(17) (a) Lacoste, R. G.; Christoffers, G. V.; Martell, A. E. *J. Am. Chem. Soc.* **1965**, *87*, 2385–2388. (b) Martell, A. E.; Motekaitis, R. J.; Smith, R. M. NIST Critically selected stability constants of metal complexes database. Version 8.0 for windows. Gaithersburg, MD: National Institute of Standards and Technology, Standard Reference Data Program, 2004.

Table 1. Protonation Constants of bp18c6 and Related Ligands and Stability Constants of Their Ln^{III} Complexes (25 °C; $I = 0.1$ M (KCl))

	bp18c6	odda[a]	oddm[b]	edta[c]
log K_1	7.41 (0.01)	8.45	7.95	10.17
log K_2	6.85 (0.01)	7.80	7.35	6.11
log K_3	3.32 (0.01)	2.90	3.03	2.68
log K_4	2.36 (0.01)			
log K_5	1.69 (0.01)			
log K_{LaL}	14.99 (0.02)	12.21		15.46
log K_{LaHL}	2.28 (0.03)			
log K_{CeL}	15.11 (0.01)	12.23	16.15	15.94
log K_{CeHL}	2.07 (0.02)			
log K_{PrL}	14.70 (0.02)	12.22		16.36
log K_{PrHL}	2.96 (0.04)			
log K_{NdL}	14.36 (0.01)	12.21		16.56
log K_{NdHL}	2.08 (0.02)			
log K_{SmL}	13.80 (0.01)			17.10
log K_{SmHL}	2.70 (0.01)	12.12		
log K_{EuL}	13.01 (0.01)	12.02		17.32
log K_{EuHL}	1.97 (0.07)			
log K_{GdL}	13.02 (0.01)	11.93		17.35
log K_{GdHL}	2.48 (0.03)			
log K_{TbL}	11.79 (0.01)	11.70		17.92
log K_{TbHL}	2.91 (0.01)			
log K_{DyL}	11.72 (0.01)	11.57		18.28
log K_{DyHL}	2.42 (0.06)			
log K_{HoL}	10.59 (0.02)	11.18		18.60
log K_{ErL}	10.10 (0.01)	11.30		18.83
log K_{TmL}	9.59 (0.01)	11.10		19.30
log K_{YbL}	8.89 (0.02)	10.90		19.48
log K_{LuL}	8.25 (0.02)	10.84	10.74	19.80

[a] Reference 8. [b] Reference 12. [c] Reference 17.

amine nitrogen atoms. A similar effect has been observed when two of the acetate groups of edta were replaced by 6-methyl-2-pyridinecarboxylate groups.[18] The third and fourth protonation steps of bp18c6 are associated to the carboxylic acid groups,[18] while the fifth protonation step probably occurs on the nitrogen atom of a pyridine unit.

Potentiometric titrations of the bp18c6 ligand have been carried out in the presence of equimolar Ln^{III} ions in order to determine the stability constants of the metal complexes. Monoprotonated forms of the bp18c6 complexes have been detected over the pH range studied for the lighter Ln^{III} ions (Ln = La−Dy), while for the heaviest Ln^{III} ions (Ln = Ho−Lu) protonated forms were not observed. The bp18c6 complexes of La^{III} and Ce^{III} show the highest log K_{ML} values among the different Ln^{III} ions, with a dramatic drop of the stability observed from Ce^{III} to Lu^{III} as the ionic radius of the Ln^{III} ions decreases. This trend is in contrast to those of most classical polydentate acyclic and macrocyclic ligands in aqueous solution, whose stability constants with Ln^{III} ions increase from La^{III} to Lu^{III} due to the increase of charge density of the metal ions (see the log K_{ML} values reported for edta in Table 1). For the largest Ln^{III} ions, the log K_{ML} values obtained for the bp18c6 complexes are comparable to those for oddm and edta and considerably higher than for odda complexes. On the other hand, with the smallest Ln^{III} ions, the stability constants of bp18c6 complexes are clearly lower than those determined for odda, oddm, and edta. Thus, the log K_{ML} values reported in Table 1 evidence an unprecedented selectivity of bp18c6 for the light Ln^{III} ions ($\Delta\log K_{ML} = \log K_{CeL} - \log K_{LuL} = 6.9$). This drop in the log K_{ML} values is 6 orders of magnitude higher than that observed for odda (1.4) and 1 order of magnitude higher than that reported for oddm (5.4).

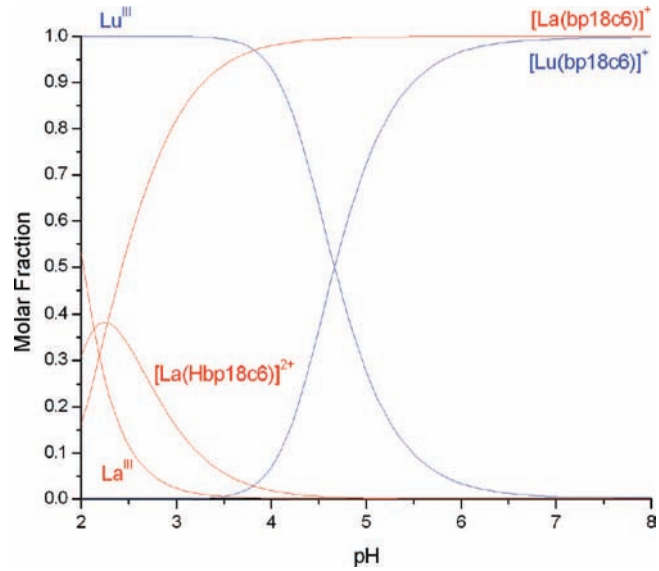

Figure 1. Species distribution of the La(bp18c6) and Lu(bp18c6) systems, 1:1 Ln^{III}/L; $[Ln^{III}] = 1$ mM, $I = 0.1$ M (KCl), 25 °C.

The species distribution diagrams for the representative La^{III} and Lu^{III} complexes are depicted in Figure 1. The diagram obtained for La^{III} shows the presence of monoprotonated complex in solution at pH < 4.5, while the dissociation of the complex occurs below pH ∼3.5. The maximum concentration of the protonated form of the complex (ca. 38%) is reached at a pH of about 2.2. The lower stability of the Lu^{III} complex is evidenced by the fact that its dissociation occurs already at pH < 7. In this case the monoprotonated complex is not formed as a consequence of the dissociation of the $[Lu(bp18c6)]^+$ complex at relatively high pH.

^{1}H and ^{13}C NMR spectra. The ^{1}H and ^{13}C NMR spectra of the diamagnetic La^{III} and Lu^{III} complexes of bp18c6 were obtained in D_2O solution at pD 8.0. The proton spectra consist of 17 signals corresponding to the 17 different proton magnetic environments of the ligand molecule (see Scheme 1 for labeling). This points to an effective C_2 symmetry of the complexes in solution that is confirmed by the ^{13}C spectra, which show 13 NMR peaks for the 26 carbon nuclei of the ligand backbone. The assignments of the proton signals (Table 2) were based upon standard 2D homonuclear COSY and NOESY experiments, which gave strong cross-peaks between the geminal CH_2 protons and between ortho-coupled pyridyl protons, and HMQC and HMBC 2D heteronuclear experiments. Although the specific CH_2 proton assignments of the axial and equatorial H7−H13 protons were not possible on the basis of the 2D NMR spectra, they were carried out using the stereochemically dependent proton shift effects, resulting from the polarization of the C−H bonds by the electric field effect caused by the cation charge. This results in a deshielding effect of the equatorial protons, which are pointing away from the Ln^{III} ion.[19,20] The bridging

(18) Chatterton, N.; Gateau, C.; Mazzanti, M.; Pécaut, J.; Borel, A.; Helm, L.; Merbach, A. *Dalton Trans.* **2005**, 1129–1135.

(19) (a) Esteban-Gómez, D.; Platas-Iglesias, C.; Enríquez-Pérez, T.; Avecilla, F.; de Blas, A.; Rodríguez-Blas, T. *Inorg. Chem.* **2006**, *45*, 5407–5416. (b) Vaiana, L.; Regueiro-Figueroa, M.; Mato-Iglesias, M.; Platas-Iglesias, C.; Esteban-Gómez, D.; de Blas, A.; Rodríguez-Blas, T. *Inorg. Chem.* **2007**, *46*, 8271–8282.

(20) González-Lorenzo, M.; Platas-Iglesias, C.; Avecilla, F.; Geraldes, C. F. G. C.; Imbert, D.; Bünzli, J.-C. G.; de Blas, A.; Rodríguez-Blas, T. *Inorg. Chem.* **2003**, *42*, 6946–6954.

Table 2. ^{1}H and ^{13}C NMR Shifts (ppm with Respect to TMS) for the La^{III} and Lu^{III} Complexes of bp18c6[a]

^{1}H	La[b]	Lu[c]	^{13}C	La	Lu
H3	7.27	7.27	C1	171.9	171.5
H4	7.76	7.76	C2	149.6	148.4
H5	7.44	7.44	C3	121.6	122.2
H7a	3.47	3.99	C4	140.3	141.2
H7b	5.10	4.59	C5	126.2	126.8
H8ax	2.28	2.84	C6	158.1	158.1
H8eq	2.65	3.58	C7	59.5	64.0
H9ax	3.39	4.10	C8	55.5	56.8
H9eq	4.00	4.49	C9	68.6	74.7
H10ax	3.51	4.13	C10	71.3	72.5
H10eq	3.99	4.33	C11	69.5	71.4
H11ax	3.57	3.84	C12	67.4	71.1
H11eq	3.90	4.12	C13	53.4	54.5
H12ax	3.65	3.27			
H12eq	4.33	3.57			
H13ax	2.47	2.42			
H13eq	3.45	2.92			

[a] See Scheme 1 for labeling; assignment supported by 2D COSY, NOESY, HMQC and HMBC experiments at 300 K and pD 8.0. [b] $^{3}J_{3,4} = 7.7$ Hz; $^{3}J_{5,4} = 7.8$ Hz; $^{2}J_{7a,7b} = 15.8$ Hz. [c] $^{3}J_{3,4} = 7.5$ Hz; $^{3}J_{5,4} = 7.8$ Hz; $^{2}J_{7a,7b} = {}^{2}J_{7b,7a} = 16.4$ Hz.

methylene protons H7a and H7b show an AB pattern at 3.47 and 5.10 ppm (La^{III}) and 3.99 and 4.59 ppm (Lu^{III}), where the larger shift for H7b probably results from the combined deshielding effects of the pyridyl ring current and polarizing effect of Ln^{III} on the C−H bond pointing away from it. The NOESY spectra give cross-peaks relating H7a and H13ax protons, while the HMBC spectra show cross peaks relating C10−H9eq and C11−H12eq, which allows a full assignment of the ^{1}H and ^{13}C NMR spectra.

The ^{13}C NMR signals due to carbons C1−C6 observed in the spectrum of the Lu^{III} complex are shifted by a maximum of 1.2 ppm with respect to their position in the spectrum of the La^{III} complex (Table 2). However, the signals due to aliphatic carbons C7−C13 experience important downfield shifts upon decreasing the ionic radius of the Ln^{III} ion from La^{III} to Lu^{III} (Figure S1, Supporting Information). Particularly important are the downfield shifts observed for C7 ($\Delta\delta = +4.5$ ppm) and C9 ($\Delta\delta = +6.1$ ppm). A similar situation is observed in the ^{1}H NMR spectra: the signals due to proton nuclei of the pyridine moieties are observed in the same position for the La^{III} and Lu^{III} complexes, while most of the signals due to aliphatic proton nuclei experiment important shifts upon decreasing the ionic radius of the Ln^{III} ion from La^{III} to Lu^{III}. These results suggest that these complexes possess different structure in solution, most likely due to a different conformation of the relatively flexible crown moiety.

The ^{1}H NMR spectra of the paramagnetic Ce^{III}, Pr^{III}, Nd^{III}, Eu^{III}, and Yb^{III} complexes of bp18c6 were also obtained in D_2O solution at pD 8.0 (Figure 2). The spectra show 17 signals, in agreement with an effective C_2 symmetry of the complexes in solution. The assignments of the proton signals (Table 3) were based upon standard 2D homonuclear COSY and line-width analysis. Indeed, the 14 ^{1}H NMR peaks due to protons 7−13 (Scheme 1) can be grouped into two different sets according to their relative line broadening, seven resonances showing considerably larger linewidths at half-height than the remaining ones (Figure 2). These two sets of signals correspond to two sets of Ln^{III}−proton distances, the broader resonances being

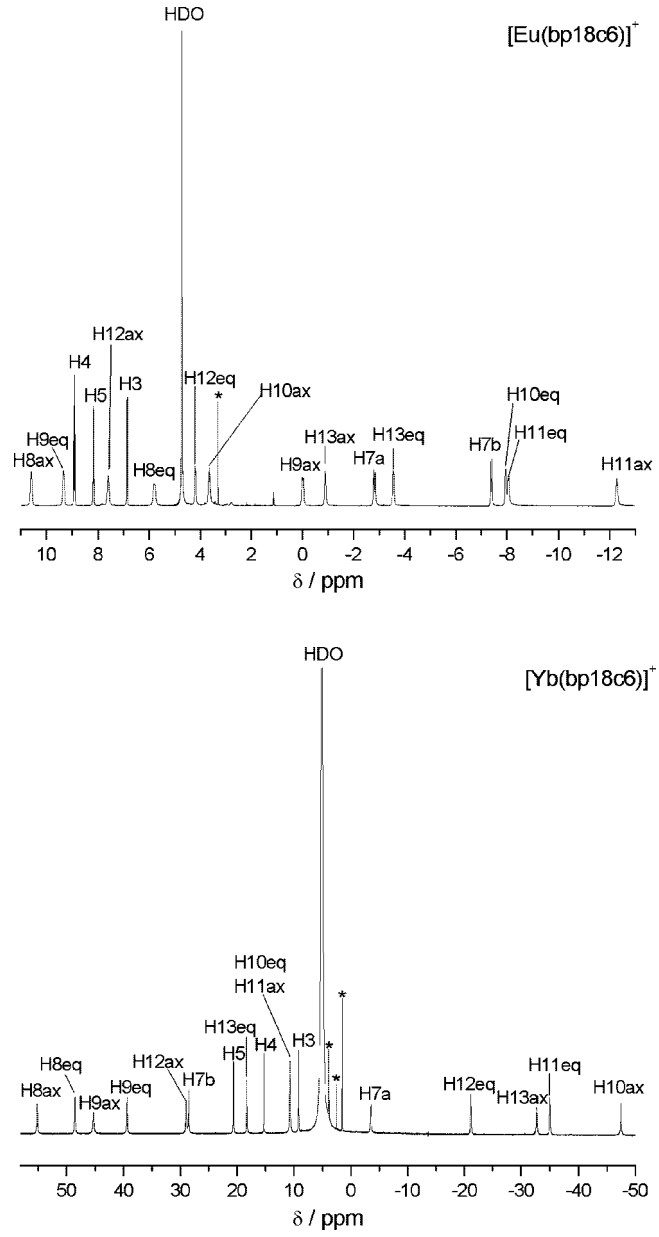

Figure 2. ^{1}H NMR spectra of the Eu^{III} and Yb^{III} complexes of bp18c6 as recorded in D_2O solution at 300 K (pD 8.0). See Scheme 1 for labeling. Diamagnetic impurities are labeled with an asterisk.

associated with the protons closer to the metal ion.[21] Thus, the broader resonances were assigned to axial protons, while the second set of signals was assigned to equatorial ones. A full assignment of the spectra was achieved by using the Shift Analysis method developed by Forsberg (see below). The ^{1}H NMR spectra of the complexes of bp18c6 with highly paramagnetic Ln^{III} ions (Tb−Tm) were also obtained in D_2O solution. However, an assignment of the spectra of these complexes was not possible due to the excessive line-broadening of many proton signals.

X-ray Crystal Structures. The solid-state structures of Gd^{III} and Yb^{III} complexes of bp18c6 have been determined by X-ray diffraction studies. Crystals were obtained by slow evaporation of solutions of the complexes prepared in situ in 2-propanol.

(21) Aime, S.; Barbero, L.; Botta, M.; Ermondi, G. *J. Chem. Soc., Dalton Trans.* **1992**, 225–228.

Table 3. ^{1}H Shifts (ppm with Respect to TMS) for Paramagnetic $[Ln(bp18c6)]^+$ Complexes Recorded in D_2O Solution at 300 K and pD 8.0 (Ln = Ce, Pr, Nd, Eu, or Yb)[a]

^{1}H	Ce^{III}	Pr^{III}	Nd^{III}	Eu^{III}	Yb^{III}
H3	10.14	13.63	8.85	6.86	8.75
H4	8.85	9.58	8.14	8.90	14.92
H5	6.60	4.76	7.48	8.17	20.31
H7a	1.78	−7.12	5.84	−2.82	−4.03
H7b	−2.01	−9.74	8.40	−7.40	28.29
H8ax	−13.98	−31.72	−12.74	10.59	55.16
H8eq	−6.48	−16.54	−1.08	5.80	48.36
H9ax	−3.53	−12.21	−5.24	−0.03	45.22
H9eq	−2.77	−7.64	−4.00	9.33	39.29
H10ax	8.70	16.37	5.40	3.65	−48.20
H10eq	4.42	9.90	5.08	−7.95	10.26
H11ax	9.51	21.16	11.60	−12.28	10.26
H11eq	8.20	14.72	8.02	−8.06	−35.75
H12ax	6.56	6.43	2.69	7.60	28.64
H12eq	6.00	6.91	8.36	4.20	−21.83
H13ax	−2.48	−13.43	12.68	−0.89	−33.19
H13eq	−1.58	−7.12	9.36	−3.54	18.01

[a] See Scheme 1 for labeling; assignment supported by 2D COSY experiments at 300 K and pD 8.0.

Attempts to obtain single crystals of the complexes from aqueous solutions were unsuccessful. The crystal of the Gd^{III} compound contains the cation $[Gd(bp18c6)]^+$, one perchlorate anion, and a 2-propanol molecule. The crystal of the Yb^{III} analogue contains the cation $[Yb(bp18c6)]^+$, three perchlorate anions, two triethylammonium cations, and a noncoordinated water molecule. Figure 3 shows a view of the complex cations, while bond distances of the metal coordination environment are given in Table 4. In the case of the $[Yb(bp18c6)]^+$ complex several carbon atoms of the macrocyclic unit are disordered into two positions, as often observed for Ln^{III} complexes with ligands based on crown-ether platforms.[20,22] In both complexes the metal ion is directly bound to the 10 donor atoms of the bp18c6 ligand, with the side arms of the ligand being placed above the plane of the macrocyclic unit, which results in a syn conformation. Likewise, the lone pair of both pivotal nitrogen atoms is directed inward the receptor cavity in an endo−endo arrangement.

The distances between the Ln^{III} ion and the oxygen atoms of the crown moiety are shorter than those between the metal ion and the pivotal nitrogen atoms, as previously observed in Ln^{III} complexes derived from 4,13-diaza-18-crown-6,[22] while the distances between the lanthanide and the donor atoms of the picolinate pendants are ca. 0.01−0.11 Å shorter than those found for 10-coordinate Gd^{III} complex of an acyclic ligand containing picolinate moieties.[18] Most of the bond distances of the metal coordination environment are shorter in the Yb^{III} complex than in the Gd^{III} analogue. However, the Yb−N1 and Yb−N2 bond distances are clearly longer than the analogous distances observed in the complex of the larger Gd^{III} ion. These results suggest a higher degree of correspondence between the binding sites offered by the ligand structure and the binding sites required by the metal ion (complementarity)[23] for the larger Gd^{III} ion, in agreement with the drop of the log K_{ML} values observed from Gd^{III} to Yb^{III} as the ionic radius of the Ln^{III} ions decreases.

The syn conformation of the ligand in the $[Ln(bp18c6)]^+$ complexes implies the occurrence of two helicities: one associated with the layout of the picolinate pendant arms (absolute configuration Δ or Λ), and the other to the six five-membered chelate rings formed by the binding of the crown moiety (each of them showing absolute configuration δ or λ).[24,25] Inspection of the crystal structure data reveals that in the Gd^{III} complex two $\Delta(\delta\lambda\lambda)(\lambda\delta\lambda)$ and $\Lambda(\lambda\delta\delta)(\delta\lambda\delta)$ enantiomers co-crystallize in equal amounts (racemate). In the notation used, the three symbols in brackets indicate the configuration of the five-membered rings formed by the coordination of a $N-(CH_2)_2-O-(CH_2)_2-O-(CH_2)-N$ unit. In the case of the Yb^{III} complex two centrosymmetrically related enantiomers are also found in the crystal lattice. The Yb^{III} complex adopts a $\Delta(\delta\lambda\lambda)(\lambda\delta\delta)$ [or $\Lambda(\lambda\delta\delta)(\delta\lambda\lambda)$] conformation taking into account

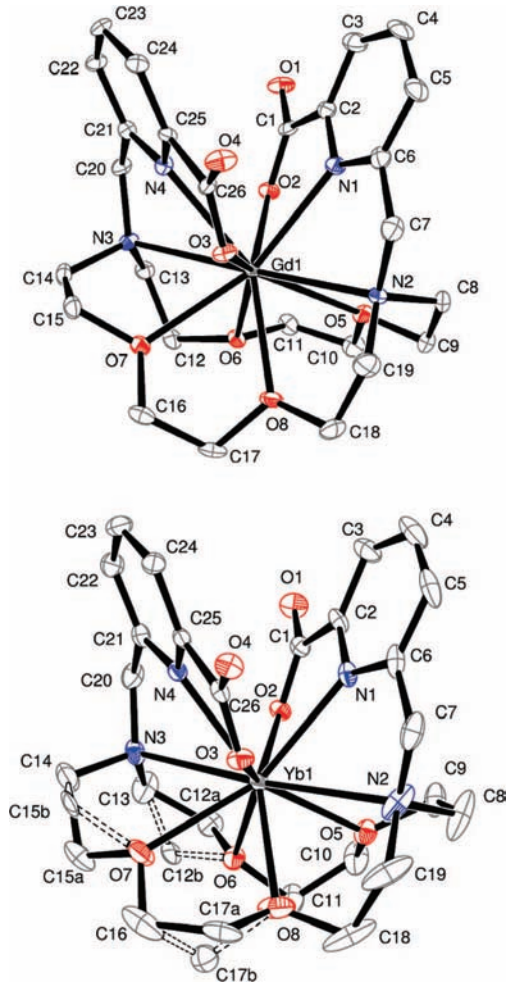

Figure 3. X-ray crystal structures of the cations $[Ln(bp12c4)]^+$ (top, Ln = Gd; bottom, Ln = Yb) with atom labeling; hydrogen atoms are omitted for simplicity. The ORTEP plots are drawn at the 50% probability level.

Table 4. Bond Lengths (Å) Obtained from X-ray Diffraction Analyses for the Gd^{III} and Yb^{III} Complexes of bp18c6 (see Figure 3 for Numbering Scheme)

	Gd	Yb		Gd	Yb
Ln1−O2	2.323(2)	2.2737(18)	Ln1−O8	2.515(2)	2.440(2)
Ln1−O3	2.360(2)	2.2526(18)	Ln1−N1	2.522(3)	2.534(2)
Ln1−O5	2.589(2)	2.4317(18)	Ln1−N2	2.768(3)	2.884(3)
Ln1−O6	2.560(2)	2.4868(19)	Ln1−N3	2.921(3)	2.865(2)
Ln1−O7	2.518(2)	2.491(2)	Ln1−N4	2.597(3)	2.499(2)

(22) Platas, C.; Avecilla, F.; de Blas, A.; Rodríguez-Blas, T.; Bastida, R.; Macías, A.; Rodríguez, A.; Adams, H. *J. Chem. Soc., Dalton Trans.* **2001**, 1699–1705.
(23) Cram, D. J.; Lehn, J.-M. *J. Am. Chem. Soc.* **1985**, *107*, 3657–3658.
(24) Corey, E. J.; Bailar, J. C., Jr. *J. Am. Chem. Soc.* **1959**, *81*, 2620–2629.
(25) Beattie, J. K. *Acc. Chem. Res.* **1971**, *4*, 253–259.

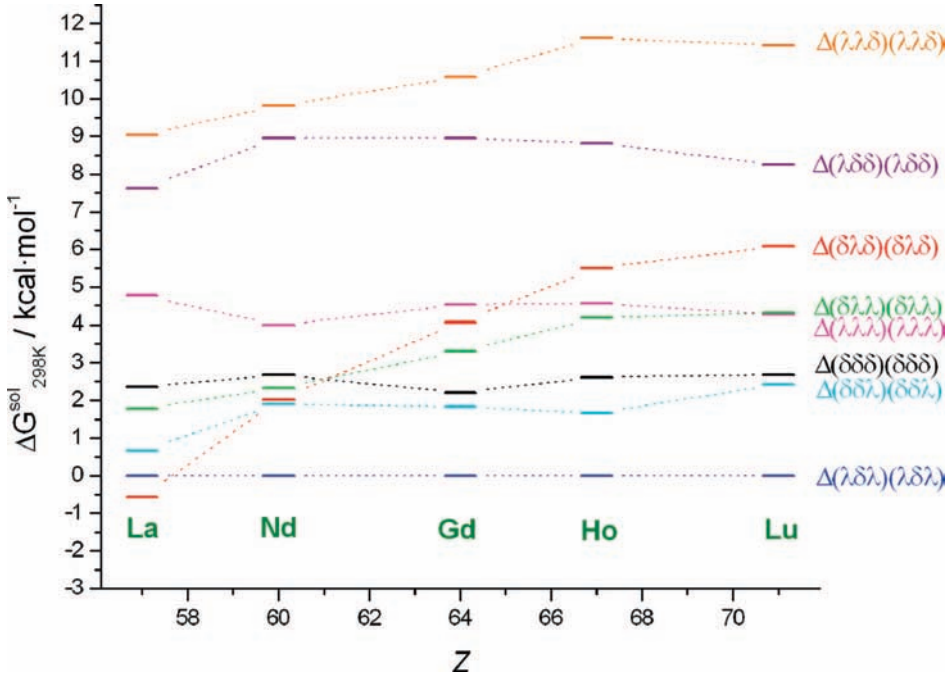

Figure 4. C-PCM relative free energies of the different diasterisomeric forms of $[Ln(bp18c6)]^+$ complexes in aqueous solution. Only those conformations showing C_2 symmetry have been included in the plot.

the positions with the highest occupation factors (C12a, C15a, and C17a, see Figure 3). The structural disorder observed for the Yb^{III} complex suggests that the flexible crown ether moiety can adopt slightly different conformations of similar energy, and thus, crystal packing forces may play an important role in the conformation observed in the solid.

DFT Calculations: Conformational Analyses. The solid-state structures of the Gd^{III} and Yb^{III} complexes of bp18c6 show that the five-membered chelate rings formed upon coordination of the crown moiety adopt a mixed-conformation in the solid state, while the ^1H and ^{13}C NMR spectra recorded for different complexes indicate a rather rigid C_2 symmetry of the complexes in solution. Thus, in order to obtain information about the structure in solution of the Ln^{III} complexes of bp18c6, as well as to understand the reasons for the unprecedented selectivity of this ligand for the largest Ln^{III} ions, the $[Ln(bp18c6)]^+$ systems (Ln = La, Ce, Nd, Gd, Ho, Yb, or Lu) were investigated by means of DFT calculations (B3LYP model). The effective core potential (ECP) of Dolg et al. and the related [5s4p3d]-GTO valence basis set was applied in these calculations. This ECP includes 46 + $4f^n$ electrons in the core, leaving the outermost 11 electrons to be treated explicitly, and it has been demonstrated to provide reliable results for several lanthanide complexes with both macrocyclic[26,27] or acyclic[13,14,28] ligands. Compared to all-electron basis sets, ECPs account to some extent for relativistic effects, which are believed to become important for the elements from the fourth row of the periodic table.

A detailed analysis of the coordinative properties of the bp18c6 ligand indicates that there are 16 possible conformations of the complexes of bp18c6 (eight enatiomeric pairs of diasteroisomers) consistent with a C_2 symmetry. Since enantiomers have the same physicochemical properties in a nonchiral environment, we have only considered in our conformational analysis the eight diasteroisomeric forms of the complexes given in Figure 4. Optimized Cartesian coordinates for the different $[Ln(bp18c6)]^+$ complexes are given in the Supporting Information. All the optimized geometries indeed show a nearly undistorted C_2 symmetry. Full geometry optimization of each conformation performed in vacuo was followed by single-point energy calculations in aqueous solution. The relative energies of the different conformations in aqueous solution are given in Table 5 and Figure 4.

Table 5. C-PCM Relative Free Energies (kcal·mol^{-1}) of the Different Diasteroisomeric Forms of $[Ln(bp18c6)]^+$ Complexes in Aqueous Solution[a]

	La^{III}	Nd^{III}	Gd^{III}	Ho^{III}	Lu^{III}
Δ(λλλ)(λλλ)	4.77	3.99	4.52	4.55	4.27
Δ(δδδ)(δδδ)	2.36	2.67	2.21	2.63	2.68
Δ(δλλ)(δλλ)	1.77	2.33	3.30	4.18	4.31
Δ(λδλ)(λδλ)	0.00	0.00	0.00	0.00	0.00
Δ(λλδ)(λλδ)	9.04	9.81	10.58	11.61	11.43
Δ(δδλ)(δδλ)	0.66	1.90	1.82	1.66	2.42
Δ(λδδ)(λδδ)	7.62	8.96	8.95	8.83	8.24
Δ(δλδ)(δλδ)	−0.57	2.01	4.07	5.49	6.07
Δ(δλλ)(λδλ)	−0.10	0.44	0.48	1.21	1.68

[a] $\Delta G^{sol} = G^{sol}_X - G^{sol}_{\Delta(\lambda\delta\lambda)(\lambda\delta\lambda)}$, and therefore, a positive relative energy indicates that the Δ(λδλ)(λδλ) conformation is more stable than the X one. The relative energies of the eight diasteroisomeric forms of C_2 symmetry are provided together with that of the conformation observed in the solid state for the Gd^{III} complex [Δ(δλλ)(λδλ)].

Our calculations predict a structural change along the lanthanide series; for the largest La^{III} ion the most stable conformation is the Δ(δλδ)(δλδ) one, while for Nd−Lu our calculations predict that the Δ(λδλ)(λδλ) form is the most stable one. The relative energies of most of the conformations of $[Ln(bp18c6)]^+$ complexes with C_2 symmetry, calculated with respect to the Δ(λδλ)(λδλ) one, are fairly constant along the lanthanide series (Figure 4). However, this is not the case for

(26) Gonzalez-Lorenzo, M.; Platas-Iglesias, C.; Avecilla, F.; Faulkner, S.; Pope, S. J. A.; de Blas, A.; Rodriguez-Blas, T. *Inorg. Chem.* **2005**, *44*, 4254–4262.
(27) Cosentino, U.; Villa, A.; Pitea, D.; Moro, G.; Barone, V.; Maiocchi, A. *J. Am. Chem. Soc.* **2002**, *124*, 4901–4909.
(28) Ouali, N.; Bocquet, B.; Rigault, S.; Morgantini, P.-Y.; Weber, J.; Piguet, C. *Inorg. Chem.* **2002**, *41*, 1436–1445.

the $\Delta(\delta\lambda\delta)(\delta\lambda\delta)$ conformation, which experiences a strong destabilization as the ionic radius of the Ln^{III} ion decreases. Indeed, the $\Delta(\delta\lambda\delta)(\delta\lambda\delta)$ conformation is the most stable one for the complex with La^{III}, but it is less stable than the $\Delta(\lambda\delta\lambda)(\lambda\delta\lambda)$ form by ca. 6.1 kcal·mol^{-1} for Lu^{III}. These results suggest a rather abrupt conformational change of the $[Ln(bp18c6)]^+$ complexes along the lanthanide series. The existence of a conformational change along the series is supported by the ^1H and ^{13}C NMR spectra of the La^{III} and Lu^{III} complexes (see above).

As shown above, the Gd^{III} complex crystallizes as a mixture of the two centrosymmetrically related enantiomers $\Delta(\delta\lambda\lambda)(\lambda\delta\lambda)$ and $\Lambda(\lambda\delta\delta)(\delta\lambda\delta)$. To evaluate the relative stability of such conformation, we have performed geometry optimizations of the $[Ln(bp18c6)]^+$ systems (Ln = La, Nd, Gd, Ho, or Lu) by using the X-ray crystal structure of the Gd^{III} complex as an input geometry. The subsequent solvated single-point energy calculation on the geometries optimized in vacuo indicates that the $\Delta(\delta\lambda\lambda)(\lambda\delta\lambda)$ conformation observed in the solid state is less stable than the lowest energy conformation with C_2 symmetry by 0.44−1.68 kcal·mol^{-1}. This result is consistent with the C_2 symmetry of the complexes in solution indicated by the NMR spectra. However, the relative energy of the conformation observed in the solid state with respect to the minimum energy conformation with C_2 symmetry is rather small. Thus, it is not surprising that crystal forces might favor the $\Delta(\delta\lambda\lambda)(\lambda\delta\lambda)$ conformation in the solid state.

Ln^{III}-Induced Paramagnetic Shifts. The binding of a ligand to a paramagnetic Ln^{III} ion generally results in large NMR frequency shifts at the ligand nuclei, with magnitudes and signs depending critically on both the nature of the lanthanide ion and the location of the nucleus relative to the metal center.[29] Thus, the analysis of the NMR spectra of Ln^{III} paramagnetic complexes can provide useful structural information in solution. For a given nucleus i, the isotropic paramagnetic shift induced by a lanthanide ion j (δ_{ij}^{para}) is generally a combination of the Fermi contact (δ_{ij}^{con}) and dipolar (δ_{ij}^{dip}) contributions:

$$\delta_{ij}^{para} = \delta_{ij}^{exp} - \delta_i^{dia} = \delta_{ij}^{con} + \delta_{ij}^{dip} \quad (4)$$

where the diamagnetic contribution δ_i^{dia} is obtained by measuring the chemical shifts for analogous diamagnetic complexes. Generally, the contact contribution quickly diminishes as the number of bonds between a given Ln^{III} and the monitored nucleus increases. We therefore initiated the analysis of the paramagnetic shifts with the assumption that they are dominated by dipolar contributions, as given by the following equation:

$$\delta_{ij}^{dip} = D_1 \frac{3\cos^2\theta - 1}{r^3} + D_2 \frac{\sin^2\theta \cos 2\phi}{r^3} \quad (5)$$

where r, θ, and φ are the spherical coordinates of the observed nucleus with respect to Ln^{III} at the origin and D_1 and D_2 are proportional, respectively, to the axial [$\chi_{zz} - 1/3(\chi_{xx} + \chi_{yy} + \chi_{zz})$] and rhombic ($\chi_{xx} - \chi_{yy}$) anisotropies of the magnetic susceptibility tensor χ. In the special case of axial symmetry the second term of eq 5 vanishes since $D_2 = 0$.

The analysis of the paramagnetic shifts to get structural information is generally initiated by assuming some structure for the complex in solution, thereby allowing the calculation of the geometric factors. A common practice is to assume that the structure in solution is the same as that determined in the solid state by X-ray crystallography, and an alternative approach is to use molecular[30,31] or quantum mechanical[32] calculations to approximate the structure of a complex. The DFT-optimized geometries of the $[Ln(bp18c6)]^+$ complexes in both $\Delta(\delta\lambda\delta)(\delta\lambda\delta)$ and $\Delta(\lambda\delta\lambda)(\lambda\delta\lambda)$ conformations were used to assess the agreement between the experimental and predicted Ln^{III}-induced paramagnetic shifts. Good fits according to the dipolar model are expected for those Ln^{III} complexes where the lowest theoretical contact contributions are expected.[29] Thus, we performed an analysis of the paramagnetic shifts observed for the Ce^{III}, Pr^{III}, and Yb^{III} complexes. The Shift Analysis program calculates the dipolar shifts defined by eq 5 in the molecular coordinate system by using a linear least-squares search that minimizes the difference between the experimental and calculated data.

The agreement between the experimental and calculated isotropic shifts for the Ce^{III} and Pr^{III} complexes obtained by using the corresponding in vacuo optimized geometries in $\Delta(\lambda\delta\lambda)(\lambda\delta\lambda)$ conformation is rather poor [$AF_j = 0.4203$ and 0.3084 for Ce^{III} and Pr^{III}, respectively]. However, a much better agreement factor is obtained for the complexes in $\Delta(\delta\lambda\delta)(\delta\lambda\delta)$ conformation [$AF_j < 0.16$, Table 6]. These results clearly confirm that these complexes present a $\Delta(\delta\lambda\delta)(\delta\lambda\delta)$ conformation in aqueous solution, in agreement with the relative energies obtained from DFT calculations. Table 6 shows the D_1 and D_2 values providing the best fit of the experimental shift values, as well as a comparison of the experimental and calculated paramagnetic shifts according to the dipolar model. As expected for nonaxial systems, the D_1 and D_2 values obtained define very large χ tensor anisotropies, with the z magnetic axis being coincident with the C_2 symmetry axis of the complexes.

In order to test the importance of the solvent effects on the DFT-optimized structures of these complexes, we have also performed geometry optimizations of the $[Ln(bp18c6)]^+$ systems (Ln = Ce or Pr) in aqueous solution. In these calculations solvent effects (water) were included by using a polarized continuum model (PCM). Our results show that the inclusion of solvent effects results in a marginal improvement of the agreement factors. Indeed, a comparison of the bond distances and angles of the metal coordination environment calculated in vacuo and in aqueous solution indicates that the inclusion of solvent effects does not substantially affect the metal coordination sphere (Table S1, Supporting Information). The inclusion of solvent effects results in the shortening of the $Ln-O_C$ bond distances (O_C = oxygen atoms of the crown moiety) by ca. 0.03−0.06 Å, while the $Ln-O_{COO}$ distances become ca. 0.06 Å longer (O_{COO} = oxygen atoms of the picolinate units). The Ln−N bond distances are nearly not affected by the inclusion of solvent effects during the geometry optimizations (<0.03 Å).

In the case of the Pr^{III} complex, a dramatic improvement of the agreement factor is obtained when the H12ax protons are excluded from the fitting procedure (Table 6). The improvement of the agreement factor upon excluding these protons from the fitting procedure may be related to (i) an important contact contribution for these nuclei and (ii) discrepancies between the structural model and the real structure of the complex in solution.

(29) Peters, J. A.; Huskens, J.; Raber, D. J. *Prog. NMR Spectrosc.* **1996**, *28*, 283–350.

(30) Di Bari, L.; Pescitelli, G.; Sherry, A. D.; Woods, M. *Inorg. Chem.* **2005**, *44*, 8391–8398.

(31) Platas-Iglesias, C.; Piguet, C.; Andre, N.; Bünzli, J.-C. G. *J. Chem. Soc., Dalton Trans.* **2001**, 3084–3091.

(32) Fernández-Fernández, M.; del, C.; Bastida, R.; Macías, A.; Pérez-Lourido, P.; Platas-Iglesias, C.; Valencia, L. *Inorg. Chem.* **2006**, *45*, 4484–4496.

Table 6. Experimental and Calculated Ln^{III}-Induced Paramagnetic ^1H NMR Shifts (ppm) for $[Ln(bp18c6)]^+$ Complexes (Ln = Ce, Pr, or Yb)[a]

	Ce^{III}			Pr^{III}				Yb^{III}			
	δ_i^{para}[b]	δ_i^{calc}[c]	δ_i^{calc}[d]	δ_i^{para}[b]	δ_i^{calc}[c]	δ_i^{calc}[d]	δ_i^{calc}[e]	δ_i^{para}[b]	δ_i^{calc}[c]	δ_i^{calc}[d]	δ_i^{calc}[e]
H3	−2.87	−2.32	−2.16	−6.36	−5.42	−5.04	−4.6	−1.48	2.76	2.21	1.76
H4	−1.09	−0.34	−0.32	−1.82	−0.73	−0.66	0.31	−7.16	−5.01	−5.33	−5.40
H5	0.84	1.51	1.43	2.68	3.98	3.86	4.13	−12.87	−11.94	−12.26	−12.04
H7a	1.69	3.07	2.90	10.59	12.44	12.00	10.66	8.02	6.68	8.07	7.69
H7b	7.11	6.05	5.91	14.84	15.64	15.42	15.23	−23.70	−22.58	−23.13	−22.22
H8ax	16.26	16.76	16.48	34.00	33.89	33.38	34.21	−52.32	−43.87	−45.77	−43.80
H8eq	9.13	8.69	8.69	19.19	18.79	19.61	19.86	−44.78	−43.06	−45.15	−42.97
H9ax	6.92	4.98	5.31	15.60	11.45	12.12	13.02	−41.80	−52.06	−51.26	−47.23
H9eq	6.77	5.62	5.68	11.64	10.15	10.15	10.68	−34.80	−29.52	−30.21	−28.24
H10ax	−5.19	−6.77	−6.99	−12.86	−15.22	−15.55	−13.95	52.33	61.19	58.83	58.34
H10eq	−0.43	−1.06	−1.22	−5.91	−4.68	−4.87	−4.47	−5.93	3.89	2.42	2.64
H11ax	−6.00	−6.07	−6.12	−17.65	−15.51	−17.14	−18.67	−6.42	3.72	1.72	−0.15
H11eq	−4.30	−4.50	−4.66	−10.82	−10.32	−10.49	−10.82	39.87	22.86	21.94	
H12ax	−2.91	−4.24	−4.34	−2.78	−6.12	−6.31		−25.37	−22.99	−26.49	−26.44
H12eq	−1.67	−1.94	−2.01	−2.58	−2.27	−2.33	−3.38	25.40	11.82	10.87	
H13ax	4.95	4.84	5.07	15.90	14.20	14.78	14.60	35.61	39.52	38.62	37.79
H13eq	5.03	4.08	4.08	10.57	12.26	12.02	11.31	−15.09	−8.12	−9.72	−9.24
D_1/ppm·Å^3		−303 ± 19	−285 ± 19		−597 ± 34	−563 ± 32	−502 ± 25		−138 ± 122	−162 ± 112	−224 ± 75
D_2/ppm·Å^3		698 ± 27	695 ± 27		1623 ± 48	1628 ± 45	1709 ± 35		4458 ± 173	4724 ± 158	4467 ± 106
AF_j		0.155	0.154		0.126	0.118	0.083		0.2590	0.2421	0.1619

[a] Calculated values were obtained by using DFT-optimized geometries showing $\Delta(\delta\lambda\delta)(\delta\lambda\delta)$ (Ln = Ce and Pr) or $\Delta(\lambda\delta\lambda)(\lambda\delta\lambda)$ (Ln = Yb) conformations (see text). [b] The diamagnetic contribution was estimated from the shifts observed for the La^{III} (Ce and Pr) or Lu^{III} (Yb) analogue; positive values correspond to shifts to higher fields. [c] Values calculated with the geometries optimized in vacuo at the B3LYP/6-31G(d) level. [d] Values calculated with the geometries optimized in aqueous solution at the B3LYP/6-31G(d) level. [e] Values calculated with the geometries optimized in aqueous solution at the B3LYP/6-31G(d) level excluding the H12ax (Pr) or H11eq and H12eq (Yb) protons from the fitting procedure.

The agreement factor obtained by excluding the H12ax protons is excellent ($AF_j = 0.0835$), and similar agreement factors were previously obtained for nonaxial Ln^{III} complexes according to the dipolar model.[33] Interestingly, poorer agreement factors between experimental and calculated shifts are often observed even when a separation of the contact contributions to the observed paramagnetic shifts has been performed.[29] This is probably due to the poor linearity observed in the contact-dipolar shift separation plots, which did not allow a reliable separation of these contributions. However, the good agreement factor obtained for the Pr^{III} complex according to the dipolar model indicate (i) that the observed paramagnetic shifts for the Pr^{III} complex are largely dipolar in origin and (ii) that the B3LYP optimized geometries are good models for the structure in solution of the complex. For the Ce^{III} complex somewhat poorer agreement factors are obtained in spite of the lower theoretical ratio of the contact and dipolar contributions.[29] This is attributed to the smaller paramagnetic shifts induced by Ce^{III} in comparison to Pr^{III} (Table 6).

The agreement between the experimental and calculated isotropic shifts for the Yb^{III} complex obtained by using the in vacuo optimized geometry in $\Delta(\delta\lambda\delta)(\delta\lambda\delta)$ conformation is very poor ($AF_j = 0.4203$), while a better agreement factor is obtained for the $\Delta(\lambda\delta\lambda)(\lambda\delta\lambda)$ conformation ($AF_j < 0.26$, Table 6). These results confirm the structural change along the lanthanide series predicted by our conformational analyses based on DFT calculations (see above). The inclusion of solvent effects results in a slight improvement of the agreement factors; a substantial improvement of the agreement factor is obtained when the H11eq and H12eq protons are excluded from the fitting procedure. However, the resulting agreement factor ($AF_j \approx 0.16$, Table 6) is substantially higher than that obtained for the Pr^{III} complex in spite of the lower theoretical ratio of the contact and dipolar contributions of Yb^{III}. Again this suggests that the paramagnetic shifts observed for these protons possess a substantial contact contribution. The contact contribution results from a through-bond transmission of unpaired spin density of Ln^{III} to the ligand nucleus.[29] The H11eq and H12eq protons are connected to the paramagnetic center through the H−C−O−Ln bonds. The same situation holds for the H12ax protons, whose exclusion from the fitting procedure leads to a very significant improvement of the agreement factor in the Pr^{III} complex. This suggests that the Ln−O bonds provide a more efficient pathway to generate contact spin density at the observed nucleus than the Ln−N bonds.

Discussion and Conclusions

Ligand bp18c6 can be obtained by using a straightforward synthetic procedure from commercially available products with an overall yield of 28%, as calculated from the pyridine-2,6-dicarboxylic acid. The stability constants of the corresponding Ln^{III} complexes (Table 1) evidence an unprecedented selectivity of bp18c6 for the light Ln^{III} ions. In order to better demonstrate the selectivity of bp18c6, we have calculated the residual free Ln^{III} concentration in solution, since the comparison of stability constants of complexes with different stoichiometry is meaningless. The inspection of the $pM = -\log [Ln^{III}]_{free}$ values across the lanthanide series confirms the discrimination capability of bp18c6. As an illustration, Figure 5 represents the evolution of pM as a function of pH for selected Ln^{III} ions. The discrimination of lanthanides by bp18c6 is clearly evidenced by the different pH where the complexes form (La, <2; Eu, ∼2.5; Lu, >4). Importantly, the formation of the Ln^{III} complexes with bp18c6 is very fast, which can allow for practical application of this ligand in separation of lanthanides. Another desirable property of the lanthanide bp18c6 complexes for application in lanthanide separation technologies is the steady variation in complex stability across the lanthanide series.[34]

In solvent extraction of lanthanide metal ions with chelating agents, lanthanides with smaller ionic radii exhibit higher

(33) Lisowski, J.; Sessler, J. L.; Lynch, V.; Mody, T. D. *J. Am. Chem. Soc.* **1995**, *117*, 2273–2285.

(34) Nash, K. L.; Jensen, M. P. *Sep. Sci. Technol.* **2001**, *36*, 1257–1282.

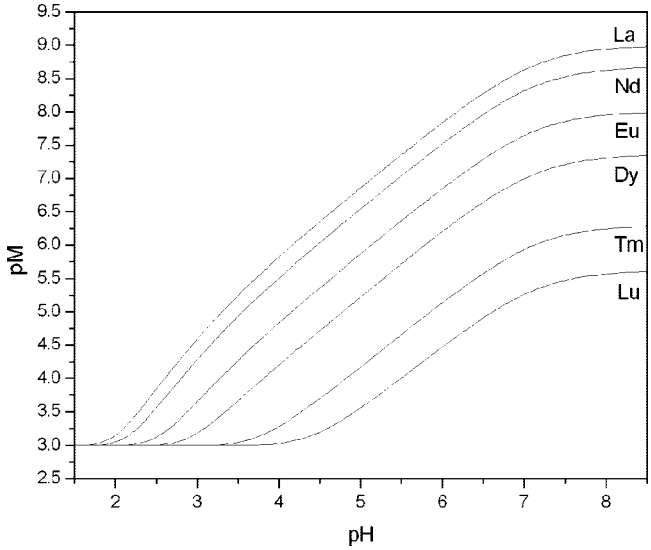

Figure 5. pM = −log $[Ln^{III}]_{free}$ as a function of pH calculated in aqueous 0.1 M KCl at 298 K with $[bp18c6]_0 = 10^{-3}$ M and $[Ln^{III}]_0 = 10^{-3}$ M.

extractability. Thus, a solvent extraction system of high selectivity could possibly be developed by combining a chelating agent in the organic phase and bp18c6 as a masking agent in the aqueous phase. Indeed, an improved separation of Ln^{III} ions has been achieved by using 18-crown-6 as ion size selective masking agent in the aqueous phase,[35] in spite of the poor selectivity that this receptor shows for the large Ln^{III} ions ($\Delta\log K_{ML} = \log K_{LaL} - \log K_{YbL} = 1.25$, as measured in propylene carbonate).[36]

The in vacuo optimized bond distances of the metal coordination environment for the relevant $\Delta(\delta\lambda\delta)(\delta\lambda\delta)$ and $\Delta(\lambda\delta\lambda)(\lambda\delta\lambda)$ conformations are given in Figure 6 (see also Table S2, Supporting Information). A careful examination of the variation of the bond distances of the metal coordination environments in $[Ln(bp18c6)]^+$ complexes provides insight into the unprecedented selectivity of this ligand for the large Ln^{III} ions. In both $\Delta(\delta\lambda\delta)(\delta\lambda\delta)$ and $\Delta(\lambda\delta\lambda)(\lambda\delta\lambda)$ conformations, most of the distances between the Ln^{III} ions and the donor atoms of the ligand decrease along the lanthanide series, as usually observed for Ln^{III} complexes as a consequence of the lanthanide contraction.[4] However, the distances between the Ln^{III} ion and the pivotal nitrogen atoms remain nearly unchanged (Figure 6). A similar situation also occurs with the distance between the Ln^{III} ion and two of the oxygen atoms of the crown moiety for the $\Delta(\delta\lambda\delta)(\delta\lambda\delta)$ conformation. The calculated $La-N_{AM}$ bond distances (N_{AM} = amine nitrogen atoms) are very similar to those previously observed for a 10-coordinate La^{III} complex with a ligand derived from 4,13-diaza-18-crown-6.[22] Thus, the interaction between the Ln^{III} ion and several of the donor atoms of bp18c6 is weakened as the ionic radius of the metal ion decreases. These results clearly indicate a better match between the binding sites offered by the ligand structure and the binding sites required by large Ln^{III} ions, which results in a dramatic drop of the complex stability as the ionic radius of the metal ion decreases. The strong destabilization of the $\Delta(\delta\lambda\delta)(\delta\lambda\delta)$ conformation with respect to the $\Delta(\lambda\delta\lambda)(\lambda\delta\lambda)$ one as the ionic

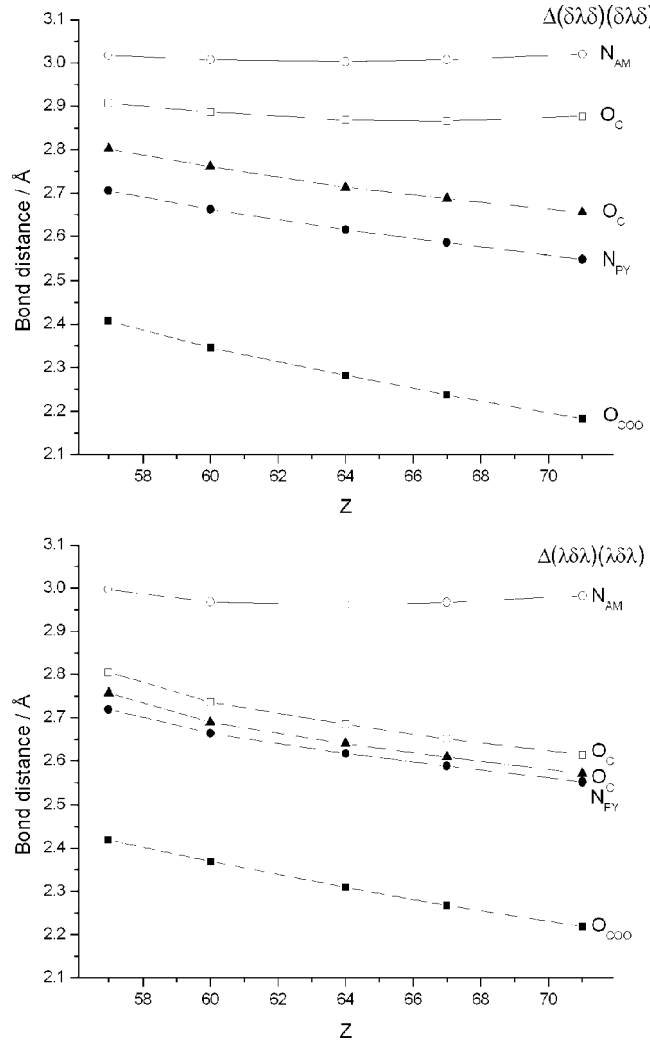

Figure 6. Variation of the calculated bond distances of the metal coordination environments for $[Ln(bp18c6)]^+$ complexes at the B3LYP/6-31G(d) level. Top, $\Delta(\delta\lambda\delta)(\delta\lambda\delta)$ conformation; bottom, $\Delta(\lambda\delta\lambda)(\lambda\delta\lambda)$ conformation. N_{AM} = amine nitrogen atoms; N_{PY} = pyridyl nitrogen atoms; O_{COO} = carboxylate oxygen atoms; O_C = crown oxygen atoms.

radius of the Ln^{III} ion decreases appears to be the result of the weakening not only of the $Ln-N_{AM}$ interactions but also of the interaction between the metal ion and two oxygen atoms of the crown moiety.

In conclusion, in this paper we have presented a new macrocyclic decadentate receptor (bp18c6) with interesting properties for application in lanthanide separation technology and analysis: (i) extremely high selectivity for the light lanthanide ions; (ii) a steady variation in complex stability across the lanthanide series; and (iii) fast formation of the Ln^{III} complexes. Theoretical calculations performed at the DFT (B3LYP) level together with experimental information on the solution structure of the complexes obtained from NMR spectroscopy indicate that (i) a conformational change occurs along the lanthanide series, the complexes with the largest Ln^{III} ions adopting a $\Delta(\delta\lambda\delta)(\delta\lambda\delta)$ conformation, and those of the smallest Ln^{III} ions a $\Delta(\lambda\delta\lambda)(\lambda\delta\lambda)$ one and (ii) the selectivity that this ligand shows for the large Ln^{III} ions is associated to a higher degree of complementarity between the binding sites offered by the ligand structure and the large lanthanides. Finally, this work also demonstrates that theoretical calculations performed at the DFT level in combination with experimental NMR

(35) Tsurubou, S.; Mizutani, M.; Kadota, Y.; Yamamoto, T.; Umetani, S.; Sasaki, T.; Le, Q. T. H.; Matsui, M. *Anal. Chem.* **1995**, *67*, 1465–1469.
(36) Almasio, M.-C.; Arnaud-Neu, F.; Schwing-Weill, M. J. *Helv. Chim. Acta* **1983**, *66*, 1296–1306.

Table 7. Crystal Data and Structure Refinement for **2** and **3**

	2	**3**
formula	$C_{29}H_{42}ClGdN_4O_{13}$	$C_{38}H_{68}Cl_3N_6\ O_{21}Yb$
MW	847.37	1224.37
space group	*Pbca*	$P2_1/c$
cryst syst	orthorhombic	monoclinic
a/Å	16.267(1)	14.8493(8)
b/Å	14.905(1)	22.4655(9)
c/Å	26.814(2)	14.9641(8)
β/deg	90	93.825(2)
V/Å^3	6501.1(8)	4980.9(4)
Z	8	4
T/K	100.0(2)	100.0(2)
λ, Å (Mo Kα)	0.71073	0.71073
D_{calc}/g cm^{-3}	1.732	1.633
μ/mm^{-1}	2.195	2.121
R_{int}	0.0881	0.0473
reflns measd	8025	13982
reflns obsd	5523	11265
R1[a]	0.0293	0.0325
wR2 (all data)[b]	0.0639	0.0713

[a] $R1 = \sum||F_0| - |F_c||/\sum|F_0|$. [b] $wR2 = \{\sum[w(|F_0|^2 - |F_c|^2)^2]/\sum[w(F_0^4)]\}^{1/2}$.

data represent a powerful tool to obtain structural information on lanthanide complexes in solution.

Experimental Section

Physical Methods. Elemental analyses were carried out on a Carlo Erba 1180 elemental analyzer and FAB-MS were recorded on a FISONS QUATRO mass spectrometer with a Cs ion-gun using 3-nitrobenzyl alcohol as matrix. IR spectra were recorded, as KBr discs, using a Bruker Vector 22 spectrophotometer. ^{1}H and ^{13}C NMR spectra were run on Bruker Avance 300 or Bruker Avance 500 spectrometers. Chemical shifts are reported in δ values. For measurements in D_2O, *tert*-butyl alcohol was used as an internal standard with the methyl signal calibrated at $\delta = 1.2$ (^{1}H) and 31.2 ppm (^{13}C). Spectral assignments were based in part on two-dimensional COSY, HMQC, and HMBC experiments.

Potentiometric Measurements. The stock solutions of $LnCl_3$ (Ln = La, Ce, Gd, and Eu) were made by dissolving Ln_2O_3 in a slight excess of concentrated HCl in double distilled water. The excess of aqueous HCl solution was removed by evaporation. The stock solutions of $LnCl_3$ for the remaining lanthanides were prepared from $LnCl_3 \cdot xH_2O$. The concentration of the solutions was determined by complexometric titration with a standardized Na_2H_2EDTA solution (H_4EDTA = ethylenediaminetetraacetic acid) using xylenol orange as indicator. Ligand stock solutions were prepared in double distilled water, and the exact ligand concentration was determined from the potentiometric titration curves with KOH.

Ligand protonaton constants and stability constants of Ln^{III} complexes (Ln = La−Lu, except Pm) were determined by pH-potentiometric titration at 25 °C in 0.1 M KCl. The samples (3−5 mL) were stirred while a constant N_2 flow was bubbled through the solutions. The titrations were carried out adding standardized KOH solution with a Methrom 702 SM Titrino automatic burette. A Metrohm 692 pH/ion-meter was used to measure pH. The H^+ concentration was obtained from the measured pH values using the correction method proposed by Irving et al.[37] The protonation and stability constants were calculated from parallel titrations with the program PSEQUAD.[38] The errors given correspond to one standard deviation.

Computational Methods. All calculations were performed employing hybrid DFT with the B3LYP exchange-correlation functional[39,40] and the Gaussian 03 package (Revision C.01).[41] Full geometry optimizations of the $[Ln(bp18c6)]^+$ (Ln = La, Ce, Nd, Gd, Ho, Yb, or Lu) systems were performed in vacuo by using the effective core potential (ECP) of Dolg et al. and the related [5s4p3d]-GTO valence basis set for the lanthanides,[42] and the 6-31G(d) basis set for C, H, N, and O atoms. In aqueous solution relative free energies of the different isomers were calculated from solvated single-point energy calculations on the geometries optimized in vacuo. Solvent effects were evaluated by using the PCM. In particular, we used the C-PCM variant[43] that employs conductor rather than dielectric boundary conditions. The solute cavity is built as an envelope of spheres centered on atoms or atomic groups with appropriate radii. Calculations were performed using an average area of 0.2 Å^2 for all the finite elements (tesserae) used to build the solute cavities. For lanthanides the previously parametrized radii were used.[44] Free energies include both electrostatic and nonelectrostatic contributions.

Analysis of the LIS Data. Lanthanide-induced paramagnetic shifts (LIS) of $[Ln(bp18c6)]^+$ complexes were calculated using the corresponding La^{III} (Ln = Ce, Pr, Nd, or Eu) or Lu^{III} (Ln = Yb) complexes as diamagnetic references. The LIS values were analyzed by using the Shift Analysis program developed by Forsberg,[45] where no assumption is made about the magnetic symmetry of the complex. The calculated strucures (DFT) of the Ce^{III}, Pr^{III}, or Yb^{III} complexes, as defined by their Cartesian coordinates with the Ln^{III} ion at the origin, were used as input structures for the analysis of the LIS values of the corresponding complexes. The agreement factors between the observed and calculated values were determined according to eq 1:[46]

$$AF_j = \sqrt{\left(\sum_i (\delta_{ij}^{exp} - \delta_{ij}^{cal})^2 / \sum_i (\delta_{ij}^{exp})^2\right)} \qquad (6)$$

where δ_{ij}^{exp} and δ_{ij}^{cal} represent the experimental and calculated values of a nucleus *i* in a given Ln^{III} complex *j*, respectively.

Chemicals and Starting Materials. 6-Chloromethylpyridine-2-carboxylic acid methyl ester was prepared as described previously.[47] All other chemicals were purchased from commercial sources and used without further purification, unless otherwise stated.

***N,N′*-Bis[(6-methoxycarbonyl-2-pyridil)methyl]-4,13-diaza-18-crown-6 (1).** 6- Chloromethylpyridine-2-carboxylic acid methyl esther (1.41 g, 7.50 mmol) and Na_2CO_3 (2.42 g, 22.83 mmol) were added to a solution of 4,13-diaza-18-crown-6 (1.0 g, 3.81 mmol) in acetonitrile (75 mL). The resulting mixture was stirred under reflux for 24 h. It was then filtered, the filtrate was concentrated and the yellow oily residue was extracted with CH_2Cl_2/water. The organic phase was dried with anhydrous $MgSO_4$ and concentrated in a rotary evaporator to give a brown oil. FAB-MS (*m*/*z*(%BPI)): 561(100) $[\mathbf{1} + H]^+$. IR: 1728 ν(C=O), 1586 ν(C=N)$_{py}$ cm^{-1}. δ_H (solvent $CDCl_3$, 295 K, 300 MHz): 7.95 (d, 2H, py, $^3J = 7.5$ Hz); 7.86 (d, 2H, py,$^3J = 7.3$ Hz); 7.76 (t, 2H, py); 3.97 (s, 6H, $-OCH_3$); 3.94 (s, 4H, $-CH_2-$); 3.60 (m, 16H, $-CH_2-$); 2.85 (m, 8H, $-CH_2-$). δ_C (solvent $CDCl_3$, 295 K, 75.5 MHz): 52.8 (primary

(37) Irving, H. M.; Miles, M. G.; Pettit, L. *Anal. Chim. Acta* **1967**, *28*, 475–488.
(38) Zékány L.; Nagypál, I. In *ComputationMethods for Determination of Formation Constants*; Leggett, D. J., Ed.; Plenum: New York, 1985; p 291.
(39) Becke, A. D. *J. Chem. Phys.* **1993**, *98*, 5648–5652.
(40) Lee, C.; Yang, W.; Parr, R. G. *Phys. Rev. B* **1988**, *37*, 785–789.
(41) Frisch, M. J.; *Gaussian03*, revision C.01; Gaussian, Inc.: Wallingford, CT, 2004.
(42) Dolg, M.; Stoll, H.; Savin, A.; Preuss, H. *Theor. Chim. Acta* **1989**, *75*, 173–194.
(43) Barone, V.; Cossi, M. *J. Phys. Chem. A* **1998**, *102*, 1995–2001.
(44) Cosentino, U.; Villa, A.; Pitea, D.; Moro, G.; Barone, V. *J. Phys. Chem. B* **2000**, *104*, 8001–8007.
(45) Forsberg, J. H.; Delaney, R. M.; Zhao, Q.; Harakas, G.; Chandran, R. *Inorg. Chem.* **1995**, *34*, 3705–3715.
(46) Davis, R. E.; Willcott, M. R. *J. Am. Chem. Soc.* **1972**, *94*, 1744–1745.
(47) Mato-Iglesias, M.; Roca-Sabio, A.; Pálinkás, A.; Esteban-Gómez, D.; Platas-Iglesias, C.; Tóth, E.; de Blas, A.; Rodríguez-Blas, T. *Inorg. Chem.* **2008**, *47*, 7840–7851.

C); 70.7, 69.8, 61.5, 54.5 (secondary C); 137.3, 126.1, 123.4 (tertiary C); 165.9, 161.4, 147.0 (quaternary C).

***N,N′*-Bis[(6-carboxy-2-pyridil)methyl]-4,13-diaza-18-crown-6 (H_2bp18c6·2HCl·2H_2O).** Compound **1** was dissolved in 6 M HCl solution (10 mL) and the solution refluxed for 40 h. After cooling to room temperature acetone was added, which resulted in the formation of a white precipitate that was collected by filtration (1.55 g, yield: 64%). Anal. Calcd for $C_{26}H_{36}N_4O_8$·2HCl·2H_2O: C, 48.7; H, 6.6; N, 8.7%. Found: C, 49.4; H, 6.0; N, 8.8%. FAB-MS (*m*/*z*(%BPI)): 547(100) $[\mathbf{L} + H]^+$. IR (KBr): 1744 ν(C═O), 1623 $\nu(C{=}N)_{py}$ cm^{-1}. δ_H (solvent D_2O, 295 K, 300 MHz): 7.93 (t, 2H, py); 7.84 (d, 2H, py, $^3J = 7.6$ Hz); 7.56 (d, 2H, py,$^3J = 7.6$ Hz); 3.85 (s, 4H, −CH−); 3.60 (m, 8H, $-CH_2-$); 3.42 (m, 8H, $-CH_2-$); 2.85 (m, 8H, $-CH_2-$). δ_C (solvent D_2O, 295 K, 75.5 MHz): 46.9, 51.1, 59.7, 61.1 (secondary C); 114.0, 117.6, 130.0 (tertiary C); 144.7, 149.7, 164.7 (quaternary C).

X-Ray Crystal Structure Determinations. Three dimensional X-ray data for [Gd(bp18c6)](ClO_4)·C_3H_8O (**2**) and [Yb(bp18c6)]-($Et_3NH)_2(ClO_4)_3$·H_2O (**3**) were collected on a Bruker X8 APEXII CCD diffractometer. Data were corrected for Lorentz and polarization effects and for absorption by semiempirical methods[48] based on symmetry-equivalent reflections. Complex scattering factors were taken from the program SHELX97[49] included in the WinGX program system[50] as implemented on a Pentium computer. The structures were solved by Patterson methods (DIRDIF99)[51] and refined by full-matrix least-squares on F^2. All hydrogen atoms were included in calculated positions and refined in riding mode, except those of the water molecule present in crystals of the Yb compound, which were located in a difference electron-density map and all the parameters fixed. Refinement converged with anisotropic displacement parameters for all non-hydrogen atoms. The Yb compound presents disorder on the crown moiety that has been solved with occupancy factors of 0.546(9) for C12A and 0.561(5) for C15A and C17A. Crystal data and details on data collection and refinement are summarized in Table 7.

Acknowledgment. A.R.-S., M. M.-I, D. E.-G., A.d.B., T.R.-B., and C.P.-I. thank Ministerio de Educación y Ciencia and FEDER (CTQ2006-07875/PPQ) and Xunta de Galicia (INCITE08ENA103005ES) for financial support. This research was performed in the framework of the EU COST Action D38 "Metal-Based Systems for Molecular Imaging Applications". The authors are indebted to Centro de Computación de Galicia for providing the computer facilities.

Supporting Information Available: ^{13}C NMR spectra of the La^{III} and Lu^{III} complexes of bp18c6, calculated (B3LYP) bond distances (Å) of the metal coordination environments for $[Ln(bp18c6)]^+$ complexes in vacuo and in aqueous solution, optimized Cartesian coordinates of the $[Ln(bp18c6)]^+$ complexes (B3LYP) in vacuo and in water and X-ray crystallographic data in CIF format for compounds **2** and **3**. Complete ref 40. This material is available free of charge via the Internet at http://pubs.acs.org.

JA808534W

(48) Sheldrick, G. M. *SADABS Version 2.10*; University of Göttingen: Göttingen, Germany, 2004.
(49) Sheldrick, G. M. *Acta Crystallogr.* **2008**, *A64*, 112–122.
(50) Farrugia, L. J. *J. Appl. Crystallogr.* **1999**, *32*, 837–838.
(51) Beurskens, P. T. Beurskens, G. de Gelder, R. Garcia-Granda, S. Gould, R. O. Israel, R. Smits, J. M. M. *DIRDIF99 program system*; Crystallography Laboratory, University of Nijmegen: Nijmegen, The Netherlands, 1999.